CHARACTERIZATION OF THE LAND SURFACE FREEZE/THAW STATE WITH SMAP-REFLECTOMETRY (SMAP-R)

Nereida Rodriguez-Alvarez, Erika Podest

Jet Propulsion Laboratory, California Institute of Technology, Pasadena, CA 91109

ABSTRACT

The use of the Soil Moisture Active Passive (SMAP) radar in received mode has allowed for a new dataset of Global Navigation Satellite System – Reflectometry (GNSS-R) measurements. GNSS-R techniques have been used for more than two decades and have proven successful perform altimetry studies and to retrieve ocean wind speed and soil moisture, monitor wetland dynamics, estimate snow depth, detect sea ice and determine sea ice types. In this paper, the SMAP-Reflectometry measurements are used to classify freeze/thaw (F/T) state over Alaska, studying the differences in the SNR signal at both V and H polarizations.

Index Terms— SMAP, reflectometry, GNSS-R, freeze/thaw state, landscapes

1. INTRODUCTION

During the past decades the use of Global Navigation Satellite System – Reflectometry (GNSS-R) has exploded. With the launch of satellite missions such as TechDemosSat-1 (TDS-1) [1] and Cyclone Global Navigation Satellite Signals (CYGNSS) [2 - 3] it has become evident that GNSS-R measurements are useful in many scenarios at a global scale. The main focus of both, TDS-1 and CYGNSS, are ocean applications, and they have consequently allowed better ocean wind studies [4 - 6]. Since the signals are also received over land surfaces, parallel studies have raised the benefit on developing land applications. With an increased temporal and spatial resolution derived from the constellation of 8 satellites, CYGNSS has benefited soil moisture [7] and wetlands dynamics [8-11] studies from the space. The polar coverage obtained from TDS-1 orbit has provided measurements over arctic sea ice and several scientific studies have proven the usefulness of the signal for altimetry [12], sea ice detection on the ocean surface [13], sea ice concentration estimates [14] and classification of different types of sea ice [15]. After the loss of the Soil Moisture Active Passive (SMAP) radar instrument, the radar was switched to 1227.45 MHz and since August 20, 2015 started collecting GPS L2C signals. The SMAP-R measurements are obtained at V and H polarization, instead of the typical left hand circularly polarized (LCHP) measurements of TDS-1 and CYGNSS. In addition to this, the SMAP antenna was designed to have high gain (36 dB) and a narrow footprint (40 km diameter), which has an impact on the signal-to-noise ratio (SNR) measured at the two polarizations. Previous studies show the use of SMAP-R signals for broad freeze/thaw (F/T) studies over the pan-Arctic region [16] and polarimetric studies over land and cryosphere [17]. Both, in [16] and [17] the information is spatially averaged at 1-degree lat/lon boxes, an area of 110 km x 50 km. The work presented here focuses on the SMAP-R received signals over Alaska at a resolution of 9 km x 9 km grid to characterize the land surface F/T state and build a retrieval algorithm that based on GNSS-R observables can help fill the gaps from other remote sensing F/T derived products. The impact of the F/T state is analyzed seasonally but accounting for different landscape classes. The signal reflected from different landcover classes clearly indicate that different signal characteristics must be considered. Section 2 defines the specifics of the SMAP-R measurements, section 3 the analysis of the data, section 4 defines the SMAP-R observables, section 5 discusses the preliminary results and section 6 summarizes the conclusions.

2. SMAP-R MEASUREMENT CHARACTERISTICS

The Earthdata website from the National Aeronautics and Space administration (NASA) provides the I/Q samples received from the SMAP radar working in receiver mode (https://earthdata.nasa.gov). The necessary processing steps are applied in order to be able to work with the data. These include filtering the data to keep only the geometries where there is a potential specular point captured and post-processing the filtered I/Q samples into delay-Doppler maps (DDM) [18, 19]. The DDM's are coherently integrated at 5 ms and incoherently integrated at 25 ms.

The reflections measured by the SMAP antenna have nearly constant incidence angle between 37.5 degrees and 42.5 degrees. This occurs because the SMAP antenna has a fixed incidence angle and a very narrow beamwidth of +/- 3 degrees at -3 dB. The scattering area over land is assumed to be much smaller than that for the ocean surface. The ocean surface has a strong incoherent component and the scattering area results in hundreds of kilometers. For land it varies. Surfaces with very low surface roughness are characterized primarily by coherent scattering such as wetlands or open water bodies such as rivers and lakes. The scattering area is reduced to between [880 m x 1290 m] to [928 m x 1450 m],

for 37.5 and 42.5 deg. incidence angle, respectively. More complex surfaces, with higher roughness show a mix between coherent and incoherent properties and as a result, the scattering area extends beyond the first Fresnel zone. However, the dominant component will remain the coherent component. For calibration purposes of the different incidence angles, we assume that most of the power comes from the first Fresnel zone. Since variation of the incidence angle is small, we expect this assumption to be accurate enough to account for the change in scattering area size. Another quality of SMAP is the high receiver antenna gain with a peak of 36 dB at 40 deg. Since the antenna is rotating, consecutive specular points are ~ 25 km apart. The GPS satellite transmitter gain is assumed to be constant since the geometry is fixed. The transmitted power is unknown, but the impact of its variations is assumed to be under 1.8 dB [18]. The observables derived from the DDMs used in this study are corrected signal-to-noise (SNR) measured at V and H polarizations, the DDM average at V and H pol, and the polarimetric ratio (PR). The corrected SNR corresponds to the measured SNR corrected for path losses and the receiver gain as well as the variation in size of the scattering area. Those observables are averaged over 9 km x 9 km grid cells during the winter months (December 2015 and January, and February of 2016) and the summer months (June, July, and August of 2016). Figure 1 shows the SNR at V polarizations for winter and summer months.

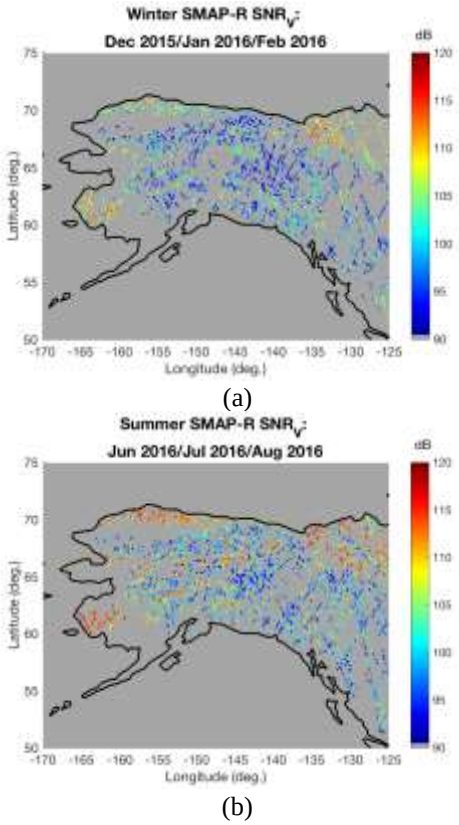

Figure 1. SMAP-R SNR at V pol averaged at 9 km x 9km grid for (a) winter months, and (b) summer months.

3. ANALYSIS OF THE DATA

Figure 1a shows the SMAP-R SNR at V-pol for winter months where several dB differences are observed over different areas. There are areas showing about 110 dB reflection peak SNR at the Yukon delta (in the western part of the state), while the northern part, around the Beaufort coastal plain, shows values around 105 dB, and the central part is predominantly around 95 dB peak SNR. We approach this wide variation in peak SNR by analyzing areas independently to determine the effect of F/T conditions on the signal according to different landcover regimes.

We initially considered the Terra and Aqua combined Moderate Resolution Imaging Spectroradiometer (MODIS) Land Cover Type (MCD12Q1) Version 6 data product, which provides global land cover types at yearly intervals (2001-2017) but determined that their classes differed from the actual land cover classes. Hence, we used a unified ecoregions map of Alaska derived in 2001 and provided by the US Geological Survey (USGS) [20], as shown in Figure 2.

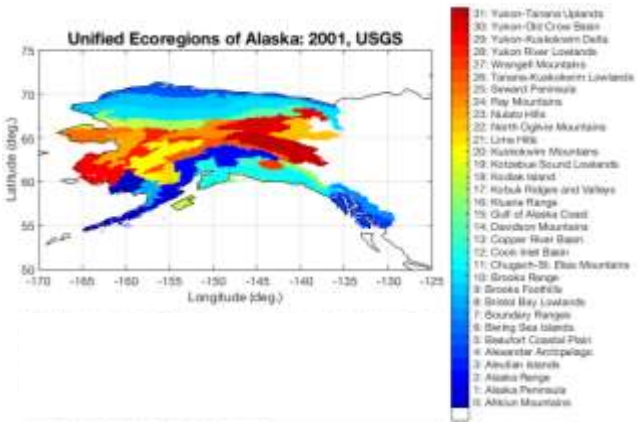

Figure 2. This ecoregion map combines the Bailey and Omernik approach to ecoregion mapping in Alaska. The ecoregions were developed cooperatively by the U.S. Forest Service, National Park Service, U.S. Geological Survey, The Nature Conservancy, and personnel from many other agencies and private organizations, [20].

By simple inspection, this ecoregion map classifies landscapes and correlates overall better with different signal variations. We have used the ecoregions map in Figure 2 as ancillary dataset in order to rigorously filter the data according to different landscape regimes that impact the signal in different ways.

Our reference dataset is the SMAP Level 3 enhanced freeze/thaw product (L3_FT_P_E). This product provides a daily classification of land surface F/T state for land areas north of 45°N derived from the SMAP radiometer, using the resolution enhanced SMAP radiometer brightness temperature, which is posted at 9 km grid spacing, as shown

in Figure 3. From the SMAP F/T product reference maps obtained for December 2015, January 2016 and February 2016 (winter months) we selected areas that were constantly frozen throughout all three months. The selected pixels were checked to ensure that they were thawed during all three summer months, from June-August 2016.

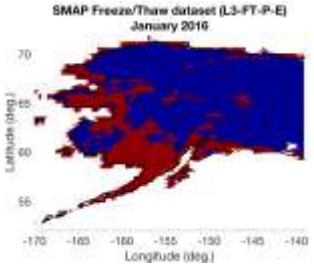

(a)

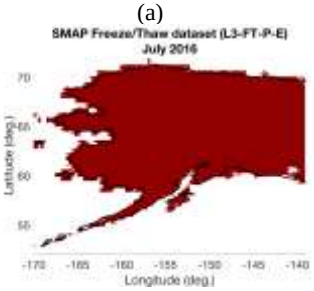

(b)

Figure 3. SMAP Level 3 enhanced freeze/thaw product (L3_FT_P_E) at 9 km x 9km grid for (a) January 2016, and (b) July 2016.

The pixels that were constantly frozen during all three winter months were overalyed on the ecoregions map in order to filter different areas, as shown in Figure 4.

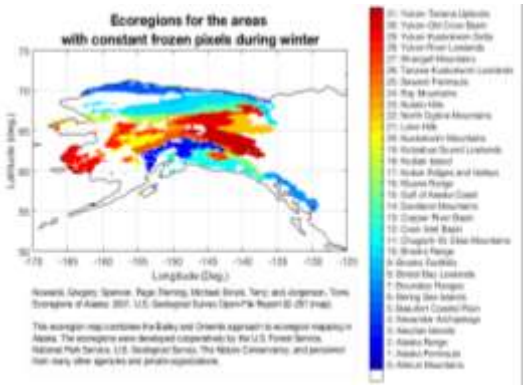

Figure 4. Ecoregions of Alaska map filtered to those areas were pixels were constantly frozen during all three winter months.

4. OBSERVABLE DEFINITION

Different GNSS-R observables computed from the SMAP-R DDMs were used in this study. We explored the impact of F/T in the following observables:

- The corrected peak SNR at V and H polarizations. Corrections were made to account for gain and path losses as well as small incidence angle differences.
- The trailing edge slope (TES) and the leading-edge slope (LES), defined as the slopes to the right and left of the maximum of the delay-waveform of the DDM.
- The DDM average (DDMA) at both polarizations, defined as the average value of the DDM bins around the specular point, 3x3 bins box considered.
- The polarimetric ratio (PR), defined as the ratio between the corrected peak SNR at V pol over the corrected peak SNR at H pol.

5. RESULTS

The difference between the observables averaged during summer and winter months using a 9 km x 9 km grid was used as an indicator of the F/T state sensitivity.

Figure 5 shows a plot of the mean SNR V pol difference between summer and winter at some of the ecoregions showed in Figure 4.

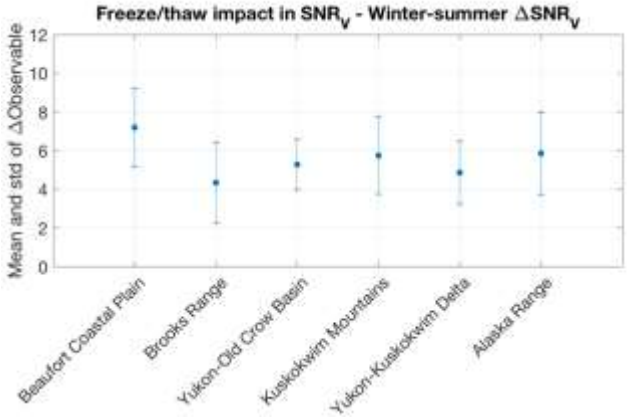

Figure. 5 Freeze/thaw impact on SNR evaluated as the difference on mean SNR_V in summer and winter.

The areas analyzed were the Yukon-Kuskokwim Delta, Beaufort Coastal Plain, Brooks Range, Alaska Range, Kuskokwim Mountains, and Yukon-Old Crow basin. The results for the different observables are numerically summarized in Table 1, which indicates that the best results are obtained for observables SNR at both H and V pol, being V pol a little more sensitive with higher μ values. Results for the DDMA at H and V pol are comparable to those obtained for the SNR. Note that the transmitted power varies slightly depending on the GPS satellite and this correction has not been applied in the current study. According to [18], after analyzing distributions of SNR across GPS satellites, biases were small and no larger than 1.8dB. The measured σ values stayed within the expected error of 1.8dB.

Table 1. Mean difference (μ) and standard deviation of the difference (σ) computed between summer and winter averaged values at a 9 km x 9 km grid for different areas according to the ecoregions map. Values are in dB.

		BEAUFORT COASTAL PLAIN	BROOKS RANGE	YUKON -OLD CROW BASIN	KUSKOKWIM MOUNTAINS	YUKON-KUSKOKWIM DELTA	ALASKA RANGE	REF. VAL
ΔSNR_H	μ	5.51	4.45	4.69	5.67	4.05	5.77	90-120
	σ	1.82	1.89	0.99	1.83	1.75	2.14	
ΔSNR_V	μ	7.20	4.34	5.28	5.74	4.86	5.85	90-120
	σ	2.02	2.08	1.30	1.99	1.62	2.13	
ΔTES_H	μ	-0.0104	-0.0306	-0.0204	-0.0360	0.0036	-0.0367	-0.26 - 0
	σ	0.0232	0.0283	0.0208	0.0271	0.0183	0.0257	
ΔTES_V	μ	-0.0249	-0.0346	-0.0177	-0.0311	0.001	-0.032	-0.26 - 0
	σ	0.0343	0.0293	0.0223	0.0220	0.0172	0.0256	
$\Delta DDMA_H$	μ	4.10	2.74	3.3619	4.09	3.03	4.13	88 - 107
	σ	1.46	1.69	0.89	1.36	1.18	1.13	
$\Delta DDMA_V$	μ	5.60	2.73	3.51	4.17	3.67	3.84	88 - 107
	σ	1.55	1.43	1.17	1.44	1.12	1.10	
PR	μ	0.31	0.22	0.17	0.24	0.15	0.13	0.3 – 1.7
	σ	0.06	0.07	0.05	0.07	0.04	0.06	

6. CONCLUSIONS

Our results indicate that the SMAP-R signal is sensitive to the F/T state of different landscapes in Alaska. The most sensitive observable is the corrected peak SNR at V polarization with, for example, mean differences of 7.2 dB and standard deviations of 2.02 dB for Beaufort coastal plain or mean differences of 5.28 dB and standard deviations of 1.30 dB for Yukon – Old crow Basin. Further analysis will include better understanding of how the different ecoregions are characterized as related to the presence of vegetation, wetlands, lakes and mountains. In addition, we will also improve the calibration to account for the differences in transmitted power between satellites.

7. ACKNOWLEDGEMENT

This research was carried out at the Jet Propulsion Laboratory, California Institute of Technology, under a contract with the National Aeronautics and Space Administration. In particular, the research on land surface freeze/thaw state was supported by the JPL internal Research and Technology Development Program. © 2018. California Institute of Technology. Government sponsorship acknowledged.

7. REFERENCES

[1] Unwin, M., et al., "Spaceborne GNSS-Reflectometry TechDemoSat-1: Early Mission Operations and Exploitation." IEEE J. Sel. Top. Appl. Earth Obs. Remote Sens., 9, 4525–4539, 2016.

[2] Ruf, C.S., et al., "The CYGNSS nanosatellite constellation hurricane mission," in 2012 IEEE International Geoscience and Remote Sensing Symposium. IEEE, pp. 214–216, 2012.

[3] Ruf, C., et al., "CYGNSS: Enabling the Future of Hurricane Prediction [Remote Sensing Satellites]," IEEE Geoscience and Remote Sensing Magazine, vol. 1, no. 2, pp. 52–67, 2013.

[4] Foti, G., et al., "Spaceborne GNSS reflectometry for ocean winds: First results from the UK TechDemoSat-1 mission". Geophys. Res. Lett., 42, 5435-5441, 2015.

[5] Clarizia, M.P., et al., "First spaceborne observation of sea surface height using GPS-Reflectometry". Geophys. Res. Lett., 43, 767-774, 2016.

[6] Clarizia, M. P., and C. S. Ruf, "Wind Speed Retrieval Algorithm for the Cyclone Global Navigation Satellite System (CYGNSS) Mission," IEEE Trans Geosci. Remote Sens., doi:10.1109/TGRS.2016.2541343, 2016.

[7] Chew, C. C., and Small, E. E. "Soil moisture sensing using spaceborne GNSS reflections: Comparison of CYGNSS reflectivity to SMAP soil moisture." Geophysical Research Letters, 45, 4049–4057.

[8] Nghiem, S. V., et al., "Wetland monitoring with global navigation satellite system reflectometry", Earth and Space Science, 2016, vol. 4, no. 1, pp. 16–39.

[9] Zuffada, C., et al., Global navigation satellite system reflectometry (GNSS-R) algorithms for wetland observations, in 2017 IEEE International Geoscience and Remote Sensing Symposium (IGARSS), 2017, pp. 1126–1129.

[10] Jensen, K.; et al., "Assessing L-Band GNSS-Reflectometry and Imaging Radar for Detecting Sub-Canopy Inundation Dynamics in a Tropical Wetlands Complex." Remote Sens. 2018, 10, 1431.

[11] N. Rodriguez-Alvarez, et al., "Characterizing Wetland Inundation with GNSS-R", MDPI Remote Sensing, (in review)

[12] Li, W.; et al., "First spaceborne phase altimetry over sea ice using TechDemoSat-1 GNSS-R signals." Geophys. Res. Lett. 2017, 44, 8369-8376

[13] Yan, Q. and Huang, W. "Spaceborne GNSS-R sea ice detection using delay-doppler maps: First results from the U.K. TechDemoSat-1 mission." IEEE J. Sel. Top. Appl. Earth Obs. Remote Sens. 2016, 9, 10, 4795-4801.

[14] Alonso-Arroyo, A.; et al., "Sea Ice Detection Using U.K. TDS-1 GNSS-R Data". IEEE TGRS 2017, 55, 9, 4989-5001.

[15] N. Rodriguez-Alvarez, et al., "Arctic sea ice multi-step classification based on GNSS-R data from the TDS-1 mission". Remote Sensing of the Environment, (in review)

[16] Chew, C., et al., "SMAP radar receiver measures land surface freeze/thaw state through capture of forward-scattered L-band signals", Remote Sensing of Environment, Volume 198, Pages 333-344, 2017.

[17] Carreno-Luengo, H., et al.; "Spaceborne GNSS-R from the SMAP mission: First assessment of polarimetric scatterometry." 4095-4098, 2017.

[18] Zavorotny, V.U. and Voronovich, A.G; Scattering of GPS signals from the ocean with wind remote sensing application. IEEE TGRS. 2000, 38, 2, 951–964. doi:10.1002/2017GL074513.

[19] Voronovich, A.G and Zavorotny, V.U.; Bistatic radar equation for signals of opportunity revisited. IEEE TGRS. 2018, 56, 4, 1959-1968.

[20] Nowacki, G, et al., "Ecoregions of Alaska: 2001." U.S. Geological Survey Open-File Report 02-297 (map).